Cement and Concrete Composites 70 (2016) 153–158

Contents lists available at ScienceDirect

Cement and Concrete Composites

journal homepage: www.elsevier.com/locate/cemconcomp

Ultra-high-ductile behavior of a polyethylene fiber-reinforced alkali-activated slag-based composite

Jeong-Il Choi [a], Bang Yeon Lee [a, *], Ravi Ranade [b], Victor C. Li [c], Yun Lee [d]

[a] School of Architecture, Chonnam National University, 77 Yongbong-ro, Buk-gu, Gwangju 61186, Republic of Korea
[b] Department of Civil, Structural, and Environmental Engineering, University at Buffalo, State University of New York, 135 Ketter Hall, Buffalo, NY 14260-4300, United States
[c] Department of Civil and Environmental Engineering, University of Michigan, Ann Arbor, MI 48109-2125, United States
[d] Department of Civil Engineering, Daejeon University, 96-3, Yongun-dong, Dong-gu, Daejeon 34520, Republic of Korea

ARTICLE INFO

Article history:
Received 9 October 2015
Received in revised form
6 April 2016
Accepted 11 April 2016
Available online 13 April 2016

Keywords:
Alkali activator
Composite
Ground granulated blast furnace slag
High ductility
Polyethylene fiber

ABSTRACT

This paper presents an experimental study of the meso-level composite properties of an ultra-high-ductile polyethylene-fiber-reinforced alkali-activated slag-based composite. Four mixtures with 1.75 vol% of polyethylene fibers were prepared with varying water-to-binder ratio. The viscosity of the matrix was controlled to ensure a uniform fiber dispersion. A series of experiments, including density, compression, and uniaxial tension tests, was performed to characterize the mechanical properties of the composite. The test results showed that the average tensile strength to compressive strength ratio of the composites was 19.8%, nearly double that of normal concrete, and the average crack width was 101 μm. It was also demonstrated that tensile strain capacity and tensile strength of up to 7.50% and 13.06 MPa, respectively, can be attained when using the proposed polyethylene-fiber-reinforced alkali-activated slag-based composites.

1. Introduction

The repair and rehabilitation of aged and deteriorated structures have become important issues in the field of construction engineering [1]. In addition, the magnitude and number of natural and man-made hazards appears to be growing. To address these issues, there is a need for technological advances that improve either the condition or performance of the members of existing structures. High-performance fiber-reinforced cementitious composites (HPFRCCs) such as high-ductile cementitious composites and ultra-high performance concrete (UHPC) have been developed to meet this technical demand [2–6]. Engineered cementitious composites (ECC) represent a unique class of HPFRCCs which are micro-mechanically tailored to feature high intrinsic tensile ductility levels with moderate amounts of fiber. Polyvinyl alcohol (PVA)-ECC shows an ultimate strain level which exceeds 4%, i.e., nearly 400 times that of concrete, as well as an ultimate strength of 4.5 MPa for composites when a moderate fiber volume fraction of 2.0% is used [7]. Recently, high-strength and high-ductility (HSHD) concrete, which is a type of UHPC, was developed. Tests of this material demonstrated a strength level similar to that of normal UHPC. The compressive strength was 166 MPa, the first-cracking strength was 8.3 MPa, and the tensile strength was 14.5 MPa. The superiority of this material was proven in tests of its tensile strain capacity, which was as high as 3.4%, which is 34 times higher than that of commercial UHPC [8,9]. In most types of HPFRCC, cement is used as the main binder. However, it is well known that the CO_2 produced by the cement industry accounts for up to 7% of global manmade CO_2 [10]. Therefore, the production of ordinary Portland cement (OPC) is considered to be one of the significant contributors to global warming.

Since the 1960s, many studies have been carried out to develop cementless slag- or geopolymer-based alkali-activated mortar and concrete and to investigate the mechanical and chemical properties of these materials in an effort to reduce the use of cement in the construction industry [11–16]. Previous studies reported that alkali-activated concrete has advantages over OPC concrete, such as high strength development at early and long-term ages, high resistance to chemical attacks and freeze-thaw cycles, and lower carbonation rates [11,13]. However, previous studies also reported that alkali-activated mortar or concrete shows brittle behavior and is susceptible to cracking, similar to OPC mortar or concrete [17,18].

* Corresponding author.
E-mail address: bylee@jnu.ac.kr (B.Y. Lee).

http://dx.doi.org/10.1016/j.cemconcomp.2016.04.002
0958-9465/

The improvement in the ductility of alkali-activated cementless mortar and concrete with self-controlled crack widths by the incorporation of the proper fibers represent another technical advancement in terms of durability and resilience as well as a 'green' material development. Lee et al. established the feasibility of developing a strain-hardening fiber-reinforced cementless composite using a mortar based on alkali-activated ground-granulated blast furnace slag (GGBS) and PVA fibers [19]. It was demonstrated that tensile strain-hardening behavior and ductility as high as 4.5% can be attained. Specifically, for three mixtures with different alkali activators and water-to-binder ratios, the compressive strength ranged from 19.4 MPa to 30.6 MPa, the tensile strain capacity ranged from 1.53% to 4.48%, the first-cracking strength ranged from 2.55 MPa to 3.87 MPa, and the tensile strength ranged from 2.83 MPa to 4.69 MPa at 28 days. Ohno and Li established the feasibility of strain-hardening fiber-reinforced fly-ash-based geopolymer composites with high tensile ductility and a tight crack width [20]. The compressive strength, tensile strength and tensile ductility of the composite were 27.6 MPa, 3.4 MPa, and 4.3%, respectively. Nematollahi et al. also developed relatively high-strength PVA-fiber-reinforced engineered geopolymer composites [21,22]. The compressive strength, tensile strength and tensile ductility of these composites were 63.7 MPa, 4.7 MPa, and 4.3%, respectively. Although it was demonstrated that a cementless alkali-activated composite reinforced with PVA fibers has tensile ductility as high as that of cement-based HPFRCC, the literature on the mechanical properties of cementless alkali-activated composites reinforced by other types of fibers is fairly limited. The polyethylene (PE) fiber has hydrophobic surface property and higher tensile strength than PVA fiber.

The purpose of this study is to improve the composite properties of fiber-reinforced alkali-activated slag-based composites by adopting PE fiber and optimizing the mixture proportion and to experimentally investigate the ultra-high tensile ductility of the new composite.

2. Materials and methods

2.1. Materials and mixture proportion

The materials and mix proportions investigated in this study are listed in Table 1. The GGBS and the alkali activator, composed of calcium hydroxide and sodium sulfate, which come in powder form to prevent quick setting, were used as binding materials. The binder type was fixed in this study. The amounts of the alkali activators, i.e., calcium hydroxide and sodium sulfate, were respectively 8.38% and 3.35% of the source material (GGBS) in terms of the mass ratio. The Blaine fineness of the GGBS used in this study was 4320 cm^2/g. The specific gravity of the GGBS was 2.92. Table 2 gives the chemical composition of the GGBS as measured in an x-ray fluorescence (XRF) analysis. The mixtures are designed to investigate the effect of the water-to-binder ratio on the properties of the composite. Aggregates, which lead to higher matrix toughness, are excluded from the mixture design for all mixtures. Using the approach suggested by Li and Li [23], optimized amounts of a high-range water-reducing admixture (HRWRA) and a viscosity-modifying agent (VMA) was used to achieve the proper rheology to ensure uniformity of the fiber dispersion. PE fiber was used as a reinforcement material in all mixtures. The properties of the PE fiber used in this study are listed in Table 3.

Table 1
Mix proportions.

Mixture	Binder	Water	HRWRA	VMA	Antifoamer	Fiber (vol%)
M26	1	0.26	0.024		0.001	1.75
M30	1	0.30	0.009		0.001	1.75
M34	1	0.34	0.004	0.0001	0.001	1.75
M38	1	0.38	0.002	0.0003	0.001	1.75

Note: All numbers are mass ratios of binder weight except fiber contents (volume fraction).

2.2. Mixing, casting, and curing of specimens

Each of the compositions described above was mixed in a Hobart mixer. Solid ingredients, including the GGBS and alkali activators, were added to the mixer, with the mixing process then continuing for approximately 3 min. Water was slowly added and the mixture was then mixed for another 3 min. Next, HRWRA and VMA, if necessary, were added to the mixer to achieve the proper viscosity of the matrix. Once a consistent mixture was reached, the fiber was gradually added, taking care to ensure a uniform fiber dispersion. The entire mixing procedure for each batch generally took 10 min. Afterwards, the mixture was cast into molds (four specimens for the uniaxial tension test and three 50-mm cubes for the cube compression test) while moderate vibration was applied. The molds were covered with plastic sheets and cured in air at room temperature (23 °C ± 3 °C) for two days. The hardened specimens were then removed from the molds and cured in water for 28 days in a laboratory room at a temperature of 23 °C ± 3 °C.

2.3. Density test

The hardened densities, ρ, were calculated by measuring the weights of the samples in air, W_{AIR}, and in water, W_{WATER}. The cubes were tested at 28 days in a water-saturated state with the excess water wiped from the surfaces.

$$\rho = \frac{W_{AIR}}{W_{AIR} - W_{WATER}} \times \rho_w \quad (1)$$

here, ρ_w is the density of water, which is assumed to be 1 g/cm^3.

2.4. Mechanical tests

The compressive strength was measured using the 50-mm cube specimens according to ASTM C109-07 [24]. To investigate the behavior of the composites under tension, uniaxial tension tests were performed using an electronic universal testing machine according to JSCE recommendations [25]. The tests were performed under displacement control with a loading speed of 0.1 mm/min, and the loading force and elongation were measured. Two linear variable differential transducers (LVDTs) were attached to both sides of the center of the tensile specimen in order to monitor the elongation. The gage length (80 mm) for each specimen was measured during the test setup, as shown in Fig. 1(b), before starting the tension test to avoid errors during the calculation of the tensile strain from the deformation. The dimensions of the cross-section within the gage length were 30 mm × 13 mm. Fig. 1 shows the specimen geometry and the test setup. In addition to the tensile stress–strain curves, the tensile strength was measured, as was the ultimate tensile strain. Four specimens were tested in order to check the variability of the performance under tension.

3. Results and discussion

3.1. Density

Table 4 presents the hardened densities of each composite as calculated by measuring the weight of three cubes in a water-

Table 2
Properties of the GGBS.

Material	Specific surface area (cm^2/g)	Density (g/cm^3)	Chemical composition (%)								
			SiO_2	Al_2O_3	Fe_2O_3	CaO	MgO	SO_3	TiO_2	K_2O	etc.
GGBS	4320	2.92	31.5	13	0.5	44.6	4.9	3.4	0.8	0.5	0.9

Table 3
Properties of the fibers.

Type of fiber	Diameter (μm)	Length (mm)	Tensile strength (MPa)	Density (g/cm^3)	Elastic modulus (GPa)
PE	12	18	2700	0.97	88

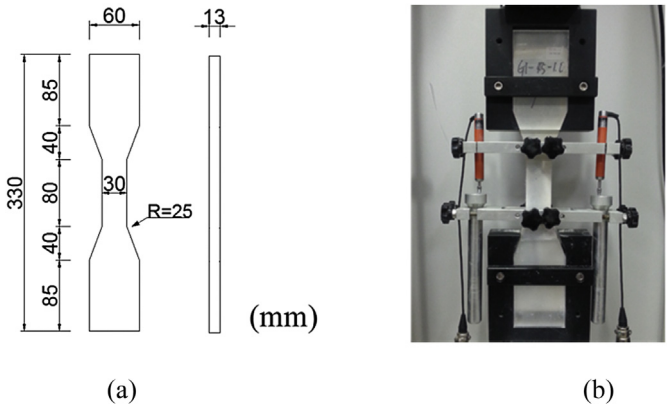

Fig. 1. Uniaxial tension test: (a) specimen geometry and (b) uniaxial tension test setup.

Table 4
Densities.

Mixture ID	Measured density (g/cm^3)
M26	2.03 ± 0.01
M30	1.99 ± 0.01
M34	1.95 ± 0.02
M38	1.89 ± 0.01

saturated state. The densities of M30, M34, and M38 were respectively 1.97%, 3.94%, and 6.90% lower than that of M26. This is attributed to the increase in the water-to-binder ratio. The theoretical densities calculated using the density of each composition and its proportion are 2.04 g/cm^3, 1.99 g/cm^3, 1.94 g/cm^3, and 1.89 g/cm^3 for M26, M30, M34, and M38, respectively. Compared to the average measured values, the error rates are less than 0.5%. These test results show that the new fiber-reinforced cementless composite was successfully processed without unintentional pores by the mixing procedure.

3.2. Compressive strength

The compressive strength of each mixture is listed in Table 5.

Table 5
Compressive strengths.

Mixture ID	Measured compressive strength (MPa)
M26	54.8 ± 1.5
M30	49.0 ± 3.2
M34	42.3 ± 2.4
M38	36.3 ± 1.0

M26, with the lowest water-to-binder ratio, showed the highest compressive strength among all mixtures. It was found that the compressive strength decreased when the water-to-binder ratio increased.

3.3. Uniaxial tensile performance

Fig. 2 shows the tensile stress and strain curves of the composites. All mixtures showed strain-hardening behavior and clear ductility with multiple cracks, in contrast to the behavior of normal concrete and fiber-reinforced concrete, which do not show multiple cracks.

The average first-cracking strength, tensile strength, and tensile strain capacity of the M26 composite were 4.87 MPa, 13.06 MPa, and 7.50%, respectively. The tensile strength of this new composite, M26, is more than double that of PE-ECC, which showed a first-cracking strength of 3 MPa, a tensile strength of 5.5 MPa, and a tensile strain capacity of approximately 6% [7,26]. The ratio of the tensile strength to the first-cracking strength of M26 was 2.68, which is 49% higher than that (1.8) of the PE-ECC.

In a comparison with the performance of the PVA-ECC, M26 has higher tensile strength by 2.9 times and a higher tensile strain capacity by 1.9 times compared to those of the PVA-ECC, whose tensile strength and tensile strain capacity were 4.5 MPa and nearly 4%, respectively [7].

The HSHD concrete showed a compressive strength of 166 MPa, a first-cracking strength of 8.3 MPa, a tensile strength of 14.5 MPa, and a tensile strain capacity of 3.4%. Although M26 has lower tensile strength compared to HSHD concrete, its ratio of the tensile strength to the compressive strength was 23.8% which is 2.7 times higher than that (8.7%) of HSHD concrete. Although it is necessary to adopt special materials such as silica fume and a filler material, a low water-to-binder ratio, and sometimes special curing conditions for UHPC, it is not necessary to adopt a special material or manufacturing process to create this new composite, as it has a moderate compressive strength. Fig. 3 shows a comparison of the tensile stress and strain curves of high-ductile composites. As shown in this figure, the new composite, M26, shows superior tensile performance, i.e., high tensile strength and ductility levels. The toughness values calculated from the tensile stress and strain curves until hardening deformation are listed in Table 6. M26 showed higher toughness by 2.7 and 1.8 times compared to the PE-ECC and HSHD concrete, respectively. Overall, the new cementless PE fiber-reinforced composite exhibited excellent tensile performance compared with those in previous studies.

The values of the first-cracking strength, tensile strength and tensile strain capacity of the four mixes are listed in Table 7. M26, which has lowest water-to-binder ratio, showed higher tensile performance in terms of the first-cracking strength, tensile strength, and tensile strain capacity. As expected, the first-cracking

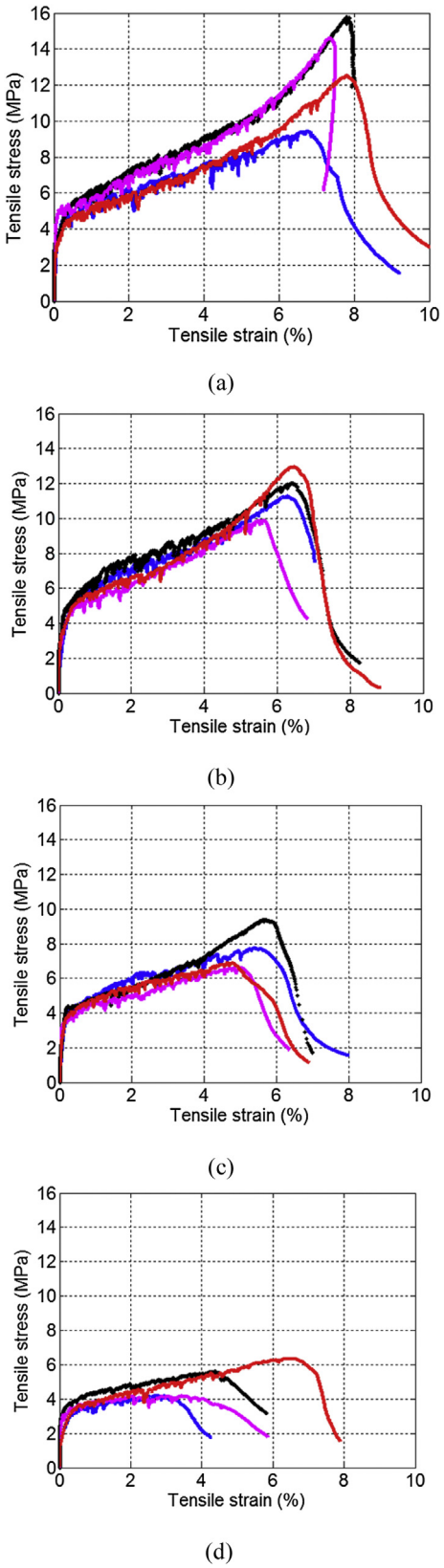

Fig. 2. Tensile stress vs. strain curve of (a) M26, (b) M30, (c) M34, and (d) M38.

strength decreased with an increase in the water-to-binder ratio. M30, M34, and M38 showed lower tensile strength levels by 12.3%, 41.5%, and 61.3%, respectively, compared to that of M26. In addition, M30, M34, and M38 showed lower tensile strain capacities by 15.6%, 28.7%, and 38.9%, respectively, compared to that of M26. Overall, it is demonstrated here that the new composite is sensitive to the water-to-binder ratio. These test results were consistent with those in previous work, which reported that the tensile behavior of PVA-fiber-reinforced alkali-activated composites is also sensitive to the water-to-binder ratio [19].

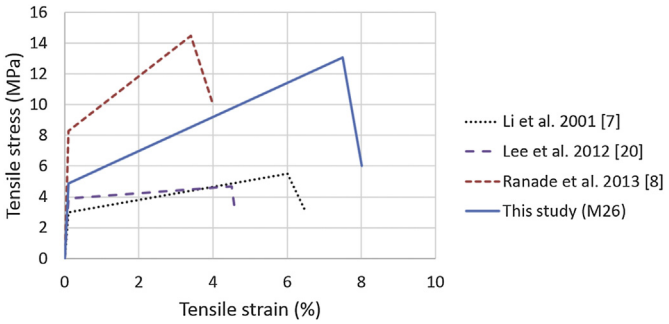

Fig. 3. Comparison diagram of the tensile stress and strain curves.

Table 6
Toughness under a uniaxial tensile load.

Composite	Toughness (MPa mm/mm)	Relative toughness
Li et al., 2001	0.0025	1.0
Lee et al., 2012	0.0019	0.76
Ranade et al., 2013	0.0038	1.5
This study (M26)	0.0067	2.7

The ratios of the first-cracking strength to the compressive strength of the new composites were 8.88%, 9.41%, 9.26%, and 9.27%, respectively, and 9.20% on average for the four types of new composites, similar to that of normal concrete. On the other hand, the ratios of the tensile strength to the compressive strength of the new composites were 23.8%, 23.4%, 18.1%, and 13.9%, respectively, and 19.8% on average for the four types of new composites. In ECC, HSHD concrete, and the new composite, the tensile strength is not a matrix property, but depends mainly on fiber bridging capacity. Hence the usual ratio of tensile strength to compressive strength (about 10%) of normal concrete would not apply to these composites.

In ultimate strength design, the tensile strength of concrete is neglected, which is mainly due to relatively lower tensile strength and fracture tensile strain compared to compressive strength and fracture compressive strain and low contribution of resistance to load. The new composite has the potential to improve the structural behavior of members or structures because it has a tensile strength up to 20% of the compressive strength as well as a high tensile strain capacity.

According to previous works on ECC micromechanics [27–30], two criteria should be satisfied in order to achieve pseudo-strain-hardening behavior based on multiple cracking. The matrix tensile cracking strength σ_c must not exceed the maximum fiber bridging strength σ_0. The strength-based criterion must control the initiation of crack propagation from the material defect sites. Another condition for pseudo strain-hardening is that the crack tip toughness J_{tip} must be less than the complementary energy J'_b, calculated from the fiber bridging stress σ versus the crack opening δ curve. Satisfaction of the energy-based criterion is necessary to assure the steady-state flat crack propagation mode and the multiple-cracking phenomenon. Kanda and Li [31] proposed the performance indices σ_0/σ_{fc} (the stress performance index) and

Table 7
Uniaxial tension test results.

Mixture ID	First cracking strength (MPa)	Tensile strength (MPa)	Tensile strain capacity (%)
M26	4.87 ± 0.46	13.06 ± 2.40	7.50 ± 0.45
M30	4.61 ± 0.26	11.46 ± 1.05	6.33 ± 0.38
M34	3.92 ± 0.37	7.64 ± 1.08	5.35 ± 0.41
M38	3.37 ± 0.34	5.06 ± 0.94	4.58 ± 1.31

J_b'/J_{tip} (the energy performance index) for the condition of saturated pseudo strain-hardening (PSH) behavior. If both of these performance indices exceed unity, PSH behavior can theoretically be achieved. However, the potential of higher tensile strain capacity increases with higher performance indices. With respect to the stress performance index, M26 showed a stress performance index of 2.68. The mixtures M30, M34, and M38 showed values of 2.49, 1.95, and 1.50, respectively. The average stress performance index for all of the mixtures was 2.16, which explains the high tensile strain capacity of all mixtures.

Fig. 4 shows the crack patterns of each mixture. Multiple microcracks with a crack spacing of less than 2.25 mm were observed. The average number of cracks, as counted manually from the unloaded specimen after the uniaxial tension test; the crack widths; and the crack spacings of four specimens for each mixture are listed in Table 8. M26, which has the maximum tensile strain capacity, showed the maximum number of cracks among all mixtures. The average number of cracks decreased with an increase in the water-to-binder ratio, which is consistent with the stress performance index. The crack width was calculated from the number of cracks and the deformation of the gauge length, during which it was assumed that all of the deformation occurred due to the opening of the crack caused by the relatively small deformation of the matrix after cracking. The average crack width of all mixtures was 101 μm. Although no constant increase was observed, M26 showed the smallest crack width among all mixtures. This is attributed to the highest strength of M26, which results in high interface frictional bonds. Previous work reported that high interface frictional bonding restrains the slippage of the fiber and is responsible for a tight crack width [32]. Crack spacings were calculated from the number of cracks and the gauge lengths. It was observed that M26 showed the minimum crack spacing and that the crack spacing increases with an increase in the water-to-binder ratio.

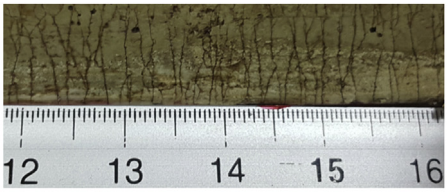

(a) M26

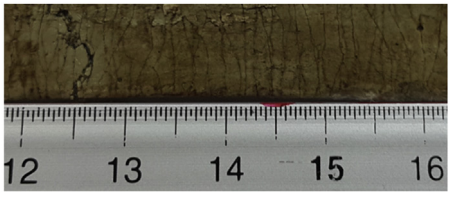

(b) M30

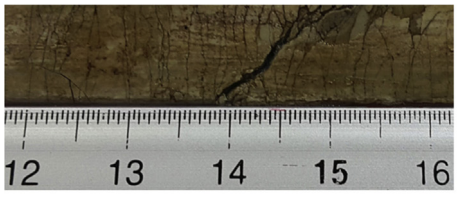

(c) M34

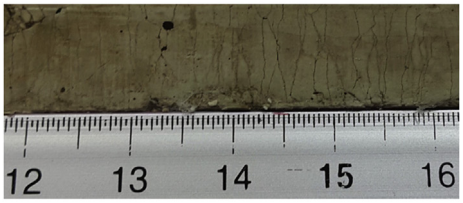

(d) M38

Fig. 4. Cracking pattern (unit of number: cm).

Table 8
Cracking pattern.

Mixture ID	Number of cracks	Crack width (μm)	Crack spacing (mm)
M26	67.3 ± 5.1	88.9	1.20
M30	47.7 ± 6.2	106.9	1.70
M34	40.3 ± 3.6	109.8	2.03
M38	36.6 ± 5.5	99.3	2.25

Although various mechanical, physical, chemical, and rheological properties should be evaluated and improved for usage as a construction material, this research is important in terms of establishing the feasibility of attaining tensile strength as high as that of UHPC as well as an extreme tensile strain capacity up to 7.5% with a moderate compressive strength, 55 MPa, in composites based on an alkali-activated GGBS-based binder.

4. Conclusion

This study investigated experimentally the tensile behavior of an ultra-high ductile PE fiber-reinforced alkali-activated GGBS composite. A series of experimental tests was carried out to investigate the mechanical properties and density levels. The following conclusions can be drawn from the current experimental results:

1. It was demonstrated that tensile strain-hardening behavior and ductility as high as 7.50% can be attained by alkali-activated composite reinforced by PE fiber. Specifically, for the four mixtures with different water-to-binder ratios, the tensile strain capacity ranged from 4.58% to 7.50%, the first-cracking strength ranged from 3.37 MPa to 4.87 MPa, the tensile strength ranged from 5.06 MPa to 7.5 MPa, and the compressive strength ranged from 36.3 MPa to 54.8 MPa at 28 days. In particular, the average ratio of the first-cracking strength to the compressive strength of the four new types of composites was 9.20%, which is similar to that of normal concrete. On the other hand, the average ratio of the tensile strength to the compressive strength of the new composites was 19.8%.

2. The M26 mixture with an alkali-activated GGBS and a water-to-binder ratio of 0.26, exhibited excellent mechanical performance compared with those of the other mixtures investigated in this study in terms of the compressive strength, tensile strength, and tensile ductility. M26 exhibited a compressive strength of 54.8 MPa, a tensile strength of 13.06 MPa, and a tensile strain capacity of 7.50%. Although the new composite, M26, has lower tensile strength compared to HSHD concrete, the ratio of the tensile strength to the compressive strength of the new composite is 23.8%, which is 2.7 times higher than that (8.7%) of HSHD concrete. Furthermore, M26 showed higher toughness by 2.7 and 1.8 times compared to the PE-ECC and HSHD concrete, respectively.
3. All mixtures showed multiple micro-cracks with a crack spacing of less than 2.25 mm. The average crack width of all mixtures was 101 μm. M26, which has the maximum tensile strain capacity, showed the maximum number of cracks, the minimum crack width, and the minimum crack spacing among all mixtures.

Acknowledgements

This research was supported by a grant (15CTAP-C097490-01) from Technology Advancement Research Program and a grant (16RDRP-B076564-03) from Regional Development Research Program funded by Ministry of Land, Infrastructure and Transport Affairs of Korean Government.

References

[1] ASCE, Report Card for America's Infrastructure, 2009.
[2] A.E. Naaman, K. Wille, The path to ultra-high performance fiber reinforced concrete (UHP-FRC): five decades of progress, in: M. Schmidt, E. Fehling, C. Glotzbach, S. Fröhlich, S. Piotrowski (Eds.), Proceedings of Hipermat 2012 3rd International Symposium on UHPC and Nanotechnology for High Performance Construction Materials, Kassel University Press, Kassel, Germany, 2012, pp. p.3–15.
[3] P. Rossi, Ultra high-performance concrete, Concr. Int. 30 (2) (2008) 31–34.
[4] H.G. Russel, B.A. Graybeal, Ultra-high Performance Concrete: A State-of-the-Art Report for the Bridge Community, Federal Highway Administration, McLean, 2013.
[5] V.C. Li, On engineered cementitous composties (ECC) – a review of the material and its applications, J. Adv. Concr. Technol. 1 (2003) 215–230.
[6] V.C. Li, Tailoring ECC for special attributes: a review, Int. J. Concr. Struct. Mater. 6 (3) (2012) 135–144.
[7] V.C. Li, S. Wang, C. Wu, Tensile strain-hardening behavior of polyvinyl alcohol engineered cementitious composite (PVA-ECC), ACI Mater. 98 (6) (2001) 483–492.
[8] R. Ranade, V.C. Li, M.D. Stults, W.F. Heard, T.S. Rushing, Composite properties of high-strength, high-ductility concrete, ACI Mater. J. 110 (4) (2013) 413–422.
[9] G. Chanvillard, S. Rigaud, Complete characterization of tensile properties of Ductal® UHPFRC according to French recommendations, in: A.E. Naaman, H.W. Reinhardt (Eds.), Proceddings of HPFRCC 4, June 2003, pp. 21–34. Ann Arbor, MI.
[10] V.M. Malhotra, Introduction: sustainable development and concrete technology, Concr. Int. 24 (7) (2001) 22.
[11] F. Pacheco-Torgal, J. Castro-Gomes, S. Jalali, Alkali activated binders: a review. Part 2—about mater and binder manufacture, Constr. Build. Mater. 22 (7) (2007) 1305–1314.
[12] A. Palomo, M.W. Grutzeck, M.T. Blanco, Alkali-activated fly ashes: a cement for the future, Cem. Concr. Res. 29 (8) (1999) 1323–1329.
[13] S. Wang, S.C. Pu, K.L. Scrivener, P.L. Ptatt, Alkali activated slag cement and concrete: a review of properties and problems, Adv. Cem. Res. 27 (1995) 93–102.
[14] F.G. Collins, J.G. Sanjayan, Workability and mechanical properties of alkali activated slag concrete, Cem. Concr. Res. 29 (3) (1999) 455–458.
[15] K.H. Yang, J.K. Song, A.F. Ashour, E.T. Lee, Properties of cementless mortar activated by sodium silicate, Constr. Build. Mater. 22 (8) (2008) 1981–1989.
[16] J.E. Oh, P.J.M. Monteiro, S.S. Jun, S. Choi, S.M. Clark, The evolution of strength and crystalline phases for alkali-activated ground blast furnace slag and fly ash-based geopolymers, Cem. Concr. Res. 40 (2) (2010) 189–196.
[17] D.P. Dias, C. Thaumaturgo, Fracture toughness of geopolymeric concretes reinforced with basalt fibers, Cem. Concr. Compos. 27 (2003) 49–54.
[18] H. Savastano Jr., P.G. Warden, R.S.P. Coutts, Potential of alternative fibre cements as building materials for developing areas, Cem. Concr. Res. 25 (6) (2003) 585–592.
[19] B.Y. Lee, C.G. Cho, H.J. Lim, J.K. Song, K.H. Yang, V.C. Li, Strain hardening fiber reinforced alkali-activated mortar – a feasibility study, Constr. Build. Mater. 37 (2012) 15–20.
[20] M. Ohno, V.C. Li, A feasibility study of strain hardening fiber reinforced fly ash-based geopolymer composites, Constr. Build. Mater. 57 (2014) 163–168.
[21] B. Nematollahi, J. Sanjayan, F.U.A. Shakh, Tensile strain hardening behavior of PVA fiber-reinforced engineered geopolymer composite, ASCE J. Mater. Civ. Eng. 27 (10) (2015), 04015001.
[22] B. Nematollahi, J. Sanjayan, F.U.A. Shakh, Strain hardening behavior of engineered geopolymer composites: effects of the activator combination, J. Aust. Ceram. Soc. 51 (1) (2015) 54–60.
[23] M. Li, V.C. Li, Rheology, fiber dispersion, and robust properties of engineered cementitious composites, Mater. Struct. 46 (3) (2013) 405–420.
[24] ASTM, Standard Test Method for Compressive Strength of Hydraulic Cement Mortars (Using 50 mm [2 in.] Cube Specimens), ASTM, 2007. C109/C109M-07.
[25] Japan Society of Civil Engineers, Recommendations for design and construction of high performance fiber reinforced cement composites with multiple fine cracks (HPFRCC), Concr. Eng. Ser. (2008).
[26] M. Maalej, V.C. Li, Flexural/tensile-strength ratio in engineered cementitious composites, ASCE J. Mater. Civ. Eng. 6 (4) (1994) 513–528.
[27] V.C. Li, C. Wu, Conditions for pseudo strain hardening in fiber reinforced brittle matrix composites, J. Appl. Mech. Rev. 45 (8) (1992) 390–398.
[28] V.C. Li, C.K.Y. Leung, Theory of steady state and multiple cracking of random discontineous fiber reinforced brittle matrix composites, J. Eng. Mech-ASCE 118 (11) (1992) 2246–2264.
[29] C.K.Y. Leung, Design criteria for pseudoductile fiber-reinforced composites, J. Eng. Mech.-ASCE 122 (1) (1996) 10–14.
[30] V.C. Li, S. Wang, Microstructure variability and macroscopic composite properties of high performance fiber reinforced cementitious composites, Probab. Eng. Mech. 21 (3) (2006) 201–206.
[31] T. Kanda, V.C. Li, Practical design criteria for saturated pseudo strain hardening behavior in ECC, J. Adv. Concr. Technol. 4 (1) (2006) 59–72.
[32] E.H. Yang, Y. Yang, V.C. Li, Use of high volume of fly ash to improve ECC mechanical properties and material greenness, ACI Mater. J. 104 (6) (2007) 303–311.